A Principled Design for Passive Light Communication

Seyed Keyarash Ghiasi
TU Delft
s.k.ghiasi@tudelft.nl

Marco A. Zúñiga Zamalloa
TU Delft
m.a.zunigazamalloa@tudelft.nl

Koen Langendoen
TU Delft
k.g.langendoen@tudelft.nl

ABSTRACT

To take advantage of Visible Light Communication (VLC) for low-power applications, such as IoT tags, researchers have been developing systems to modulate (backscatter) ambient light using LC shutters. Various approaches have been explored for *single-pixel* transmitters, but without following a principled approach. This has resulted in either relatively low data rates, short ranges, or the need for powerful artificial light sources. This paper takes a step back and proposes a more theoretical framework: ChromaLux. By considering the fundamental characteristics of liquid crystals (birefringence and thickness), we demonstrate that the design space is way larger than previously explored, allowing for much better systems. In particular, we uncover the existence of a transient state where the switching time can be reduced by an order of magnitude without lowering the contrast significantly, improving both range and data rate. Using a prototype, we demonstrate that our framework is applicable to different LCs. Our results show significant improvements over state-of-the-art single-pixel systems, achieving ranges of 50 meters at 1 kbps and with bit-error-rates below 1%.

CCS CONCEPTS

• **Computer systems organization** → **Embedded and cyber-physical systems**; • **Networks** → **Physical links**.

KEYWORDS

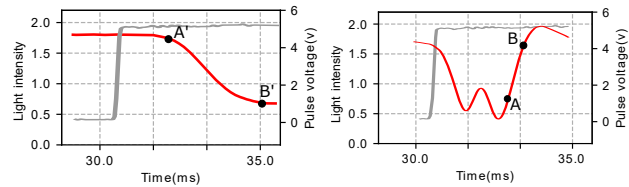visible light communication, backscattering, liquid crystal displays

1 INTRODUCTION

The ever-growing demand for wireless communication has prompted researchers to look for bandwidth beyond the traditional radio-frequency spectrum. During the last decade, the visible light spectrum has gained significant attention because it is open, free, and wide. Nowadays, any object with an LED can be transformed into a wireless transmitter, and a wide range of novel applications have

(a) State of the art　　　**(b) ChromaLux**

Figure 1: Key Insight: Existing studies assume that the transition between the end-states of liquid crystals is monotonic, which leads to symbols that have a high contrast, but a low bandwidth (like A' and B'), or the opposite trade-off. Based on first principles, ChromaLux exposes a transient state where symbols can have a high contrast *and* bandwidth (like A and B).

been developed, from the design of a new generation of toys [20] and indoor positioning systems [11] to human sensing [13].

Visible light communication (VLC) is a significant advancement, but it has a major drawback: the power consumption is high because it requires turning on LEDs, which is not the most energy efficient way of communication. To overcome this issue, researchers have proposed the use of liquid crystal (LCs) cells to modulate existing ambient light. LC cells are devices that can block or allow the passage of ambient light using very little power (μW). Several notable contributions have been made in this domain. Some studies used slow-switching LCs as *single-pixel* transmitters[1], which attain data rates ranging from a few bits per second [9, 14, 27] to 1 kbps [6, 26]. Other studies developed advanced systems using faster-switching LCs with *multi-pixel/sensor* transmitters that can achieve 1 kbps [22] and 8 kbps [25] at different ranges.

All these advances are valuable, but they have been working under the assumption that LCs only provide a monotonic change in light intensity when they transition between their opaque and translucent states. That assumption has constrained the design space of researchers, who have to choose between using (i) the end states (opaque and translucent) to modulate light, providing high contrast but low bandwidth [9, 27], or (ii) intermediate points in the transient (monotonic) state, which provides a higher bandwidth but low contrast [6, 26].

Building upon the fundamental physical properties of LCs, we design single-pixel transmitters with a non-monotonic transient state. This non-monotonic property allows us to modulate light using symbols that have a high switching speed *and* good contrast. This key insight, depicted in Figure 1, allows us to increase the bandwidth of long-range links by an order of magnitude. Overall,

---

[1]The surface of an LC cell can be seen as a single (big) pixel modulating ambient light. Multi-pixel transmitters use more than one LC surface (pixel), which helps to increase the data rate of the system.
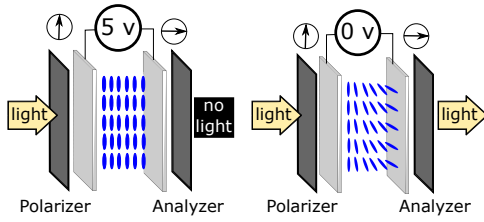
Figure 2: The operation of a liquid crystal cell.

(a) Single frequency light   (b) White light

Figure 3: The effect of birefringence on crystals

our work, dubbed ChromaLux, makes the following contributions to the area of passive communication with visible light:

1) Expose a yet unexploited transient state [section 3]. Based on the fundamental physical properties of LCs, we show that the modulation process does not need to be constrained to the simple monotonic function used in the state-of-the-art. By placing multiple cells in series, we uncover a broader modulation spectrum that contains a transient state with multiple peaks and valleys. The extremes in this transient state provide high contrast and fast switching, which we exploit to increase the channel capacity.

2) Propose a constellation diagram for single-pixel transmitters [section 4]. Contrary to traditional VLC, where there is a well-established methodology to design LED transmitters, there is no theoretical framework for passive VLC. Based on first principles, we propose a constellation diagram to obtain foundational guidelines for the design of our single-pixel LC transmitter. Our framework allows us to theoretically substantiate the need (i) to use an optimal number of LCs to maximize the channel's performance and (ii) to use symbols on a particular region of the transient state.

3) Design a novel modulation scheme [section 5]. The transient state allows exploiting symbols with high contrast and switching speed, but it is unstable and standard modulation techniques based on amplitude, frequency or phase shift keying cannot be implemented. To enable a stable wireless link, we propose a novel duty-cycling method to modulate bits based on a 3-level voltage input.

4) Evaluate our platform with artificial and natural ambient light [section 6 and section 7]. We built a proof-of-concept platform and tested it with both artificial and natural ambient light. Our results show that we can achieve a 50-meter range with low sunlight conditions (3-6 klux) with a data rate of 1 kbps and a BER below 1%. Compared to other studies, we increased the range by a factor of 20 and the transmission speed by a factor of 10. More importantly, to showcase the general validity of our approach, we evaluate two different liquid crystals and demonstrate that both increase their bandwidth by an order of magnitude.

2 BACK TO THE BASICS

To squeeze the best performance (data rate, BER, range) out of readily available LC shutters, it is important to have a good understanding of the underlying physics.

2.1 An overlooked feature: birefringence

First, we describe the basic operation of LCs, and then, we focus on the role of changes in birefringence, an important LC property that has not been considered thus far for backscatter communication.
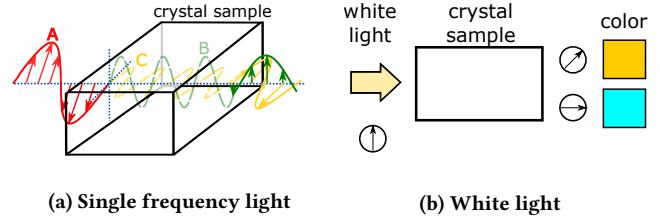
The basic operation of LCs is depicted in Figure 2. Several studies describe the inner-workings of LCs [5]. Thus, we only provide a succinct explanation. First, the incident (incoming) light is polarized by a polarizing film. Then, this polarized light enters an LC cell. If no voltage is applied on the cell, the thin layer of crystals rotates the polarization plane of the incident light by 90°, and if a voltage is applied, the polarization direction remains unchanged. A second polarizer, called the *analyzer*, either blocks or permits the passing of light depending on its alignment with the polarization direction of the outgoing light.

Refraction and birefringence The changes between translucent and opaque states is well-studied in backscatter communication, but the fact that these changes are related to birefringence has been largely overlooked, limiting the potential of LCs. In transparent materials, light travels slower than in free space. The ratio of this reduced speed with respect to c is called the *refractive index (n)*. Some materials, such as most crystals, have different different indices n for different polarization angles of light [8]. The highest and lowest values of n are important because they allow calculating the refraction index for any polarization angle. These materials are called birefringent because of these two values. An example is presented in Figure 3a. Upon entering the material, a polarized light ray (A–red) is divided into two orthogonal components along the axes of maximum and minimum of n, each traveling at a different speed, one fast (B–green) and the other slow (C–yellow). The birefringence parameter, denoted as Δn, is the difference between the refractive index of the fastest and the slowest axis of the material: $\Delta n = n_{fast} - n_{slow}$.

Due to the different changes in speed, the two rays leave the crystal with a different phase. If instead of assuming a single-frequency ray (color), we consider polarized white light (all colors), each color will end up with a different change in phase. The naked human eye perceives these out-of-phase signals as white light, but if we use an analyzer, as in Figure 3b ,we will see different colors depending on its orientation. For ChromaLux, the various changes in phase caused by birefringence are key because they allow for fast transitions with high contrast.

2.2 Birefringence in liquid crystals

Material scientists have developed numerous methods to study the properties of crystals. Consider a *solid* crystal that is sandwiched between two orthogonal polarizers. When white light enters this structure, only a certain color exits, depending on the birefringence b and thickness d of the crystal [28]. These colors are captured by the so-called Michel-Lévy chart, shown in Figure 4. In this chart, a radial line corresponds to the birefringence of a crystal and a horizontal line to its thickness (measured in nm). Thus, for a solid
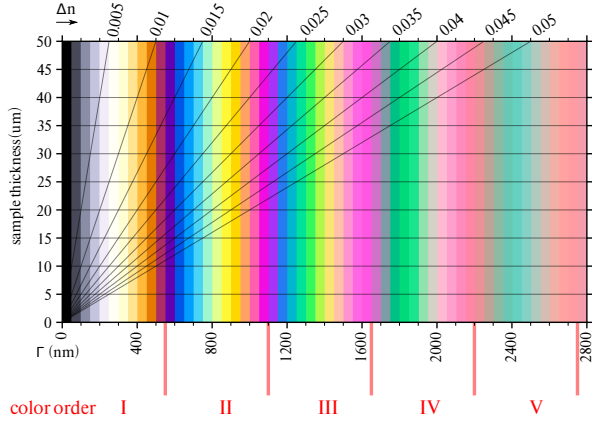
Figure 4: Michel-Levy chart [4]. The radial lines represent the birefringence values (Δ*n*, numbers on the top), and the plot shows how the color (horizontal axis) varies with the width (vertical axis). By convention, each 550 nm of path difference is named *order* and ends with a shade of magenta.

crystal, the color output is captured by the intersection of a radial and horizontal line.

What sets *liquid* crystals apart is that their birefringence changes with an external electric field. Every voltage within their operational range leads to a different birefringence value. In the Michel-Lévy chart, an LC cell is represented by two radial lines and a horizontal line (thickness). The two radial lines represent the max and min birefringence of the crystal, and there is an inverse non-linear relation between the applied voltage and the birefringence. When the voltage is decreasing, the birefringence increases covering all the spectrum within the two radial lines. That covered spectrum determines the LCs transient phase. For example, a crystal with a 25 μ*m* thickness and Δ*n*'s of 0.005 and 0.015, would have a spectrum between gray and yellow.

2.2.1 Putting the Michel-Lévy chart in the context of backscatter communication. The birefringence and thickness of typical LC shutters are chosen to cover only a narrow high-contrast region between a dark and a light color in the Michel-Lévy chart, and several studies exploited that region to modulate information (discussed in section 8). To the best of our knowledge, no prior research has connected the fundamental physical properties of LCs with backscatter communication. To formulate a theoretical framework, we build upon the equation used to create the Michel-Lévy chart, which expresses the fraction of light L that leaves the analyzer for incoming light with wavelength λ:

$$L(\Gamma, \lambda) = sin^2(\frac{180° \times \Gamma}{\lambda}) \tag{1}$$

where Gamma (Γ) is known as the *path difference*, which combines the main properties of the crystal, birefringence (Δ*n*) and thickness (*d*), on a single parameter.

$$\Gamma = \Delta n \times d \tag{2}$$

By summing over all frequencies in the visible light spectrum, one can obtain the resulting color coming out of the analyzer.

It is important to note that this equation only captures the most common LC configuration, where the angle between the polarizer
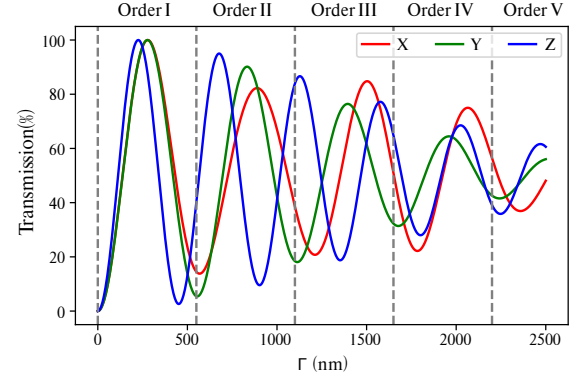

Figure 5: Theoretical color response of a liquid crystal.

and analyzer is 90°. For details on the more general equation, please refer to [17].

2.2.2 Color sensors and the theoretical response of liquid crystals. ChromaLux's approach requires decomposing light into its color components. For this task we utilize color sensors, which are simple single-pixel receivers. They can be seen as photodiodes with inexpensive color filters in front of them. There are multiple types of color sensors, and we decided to use a type called *true color* sensor because it mimics the human perception of color. The reason for that choice is that the Michel-Lévy chart is also designed to capture people's perception of colors, and hence, our sensor (empirical experiments) will be in agreement with the theoretical results (Equation 1). When referring to the output of a true-color sensor, we will follow the convention of using (X,Y,Z) coordinates, which are a transformation of the well-known (R,G,B) space.

Decomposing light into different color channels allows us to have a deeper look into the Michel-Lévy chart. Using Equation 1, we show a sample theoretical response in Figure 5, where the path difference (Γ) of a crystal gradually increases. To construct this plot, we generated (Γ, λ) tuples using Equation 1. Γ values were selected from 0 to 2500 nm, and λ values were selected from the visible light spectrum. Then, the amplitudes of wavelengths in the output light were converted to (X, Y, Z) values [17]. Initially, all channels start with zero intensity (black), then the channels increase their values in a rather synchronized manner up to the first peak (white). After that, the channels get out-of-phase, leading to the range of colors observed in the Michel-Lévy chart.

Note that the theoretical response is time-independent; it is a function of Gamma (Γ), which in turn is a function of the birefringence (Equation 2). In practice, we have to take into account the time-dependent characteristics of LC cells. Next, we analyze The empirical response of LCs and their ability to increase the bandwidth of the system.

3 SPECTRUM ANALYSIS

Based on the prior section, we know that LCs can be designed to oscillate between any two colors in the Michel-Levy chart. A designer only needs to select the appropriate birefringence values (radial lines) and thickness (horizontal line) for the liquid crystal layer. We designed a simple setup using a flashlight and a color sensor to measure the spectrum of single and multiple LC cells. The cells were placed in series between a polarizer and an analyzer
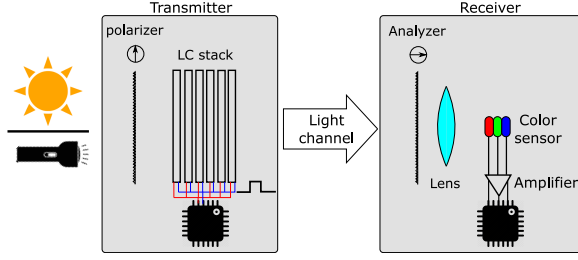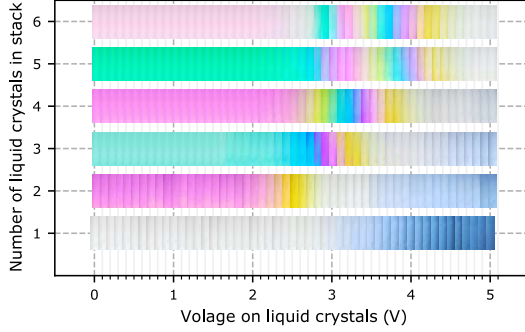
Figure 6: Setup to measure the color spectrum

Figure 7: Color spectrum for different number of cells.

(a) Falling pulse

(b) Rising pulse

Figure 8: Transition state for a single cell.

with orthogonal directions, as shown in Figure 6, and different voltage levels were applied. It is important to highlight that off-the-shelf LCs available in the market do not provide data sheets with detailed optical characteristics, but a deep understanding of those characteristics is fundamental to define a complete design space.

The derivation of our framework (section 3-5) focuses on a popular Twisted-Nematic crystal used for 3D glasses that has been explored in previous backscattering studies [1], but to demonstrate the generality of our approach, we also utilize our framework to improve the performance of a different LC shutter in section 7.

3.1 The single-cell case

To see the color spectrum of an LC stack, we place from one to six cells between a polarizer and an analyzer and change the DC voltage on the stack. We sweep the DC voltage in steps of 0.1 volts and take pictures of the output light at each step to get Figure 7. The bottom row of that figure depicts the color spectrum for a single cell when different *static* DC voltage levels are applied. As expected, the spectrum covers the dark to white transition in the first order region of the Michel-Levy chart. *The important observation from this result is that while most backscattering studies exploited this spectrum, they overlooked the fact that this transition is due to the change in the cell's birefringence value.* If, instead of using *static* voltage values, we use *dynamic* voltage pulses, we obtain the time response of the cell. Figure 8 shows the time response of a single cell when we apply falling and rising pulses between 0 and 5 V. The fact that the three channels are in phase, and have the same intensities[2], is what causes the monotonic change in the spectrum. Given that

the most popular application of LC cells is as light shutters, it makes sense to design cells whose only purpose is to oscillate between the translucent (white) and opaque (dark) states.

This monotonic behaviour has been exploited for backscatter communication in two main ways: (i) by using the end values in the steady states to encode data [9, 27], which maximizes the contrast (SNR) but at the cost of reducing the switching speed (bandwidth); or (ii) by using intermediate values, which has the opposite trade-off, lower contrast but higher switching speeds [6, 26].

The important take-away is that, to obtain that monotonically decreasing behaviour in the black/gray/white scale, manufacturers produce crystals with birefringence values and thicknesses that only cover a *very specific and narrow* portion of the theoretical response in Figure 5: the Gamma range between 0 and 250.

3.2 The multi-cell case

To increase the modulation spectrum of an LC, we need to increase its thickness or use a broader range of birefringence values. Unfortunately, the thickness and birefringence values of liquid crystals are fixed and determined during the manufacturing process. To expand the modulation spectrum, we stack multiple cells to increase the thickness of the crystal layer. In the Michel-Levy spectrum, our approach translates to using a higher horizontal line while maintaining the same radial lines.

The top five rows of Figure 7 depict the spectrum obtained with static voltages after stacking multiple cells. Since we are increasing the thickness, the color spectrum shifts to the right of the Michel-Levy chart. For example, the configuration with two LCs covers most of the first order, and the configuration with six LCs covers from the middle of the first order until the third order. Note that at low voltages (below 2 V) there are no color transitions. This occurs because the minimum operating voltage of our cells is around 1.4 V. Below that voltage, the cell does not change its state. That minimum voltage is known as the Fréedericksz threshold [10].

Next, we will see why transient states with frequent color transitions are beneficial for ChromaLux. Figure 9 depicts the time response for falling pulses when we stack 2, 4, and 6 cells. We focus on the falling pulses because they are known to be the main bottleneck in backscatter communication[3]. These time responses provide two important insights.

First, the increased spectrum exposes a non-monotonic *transient state* with considerable levels of contrast. When we increase the

---

[2]It is important to recall that the XYZ space has different ranges for each channel. For example, in the RGB space the range is the same for all channels [0,255], which means that white light is represented with all channels having the same values (255, 255, 255); but white light in the XYZ space is represented with non-homogeneous levels: (0.9642, 1.0000, 0.8252).
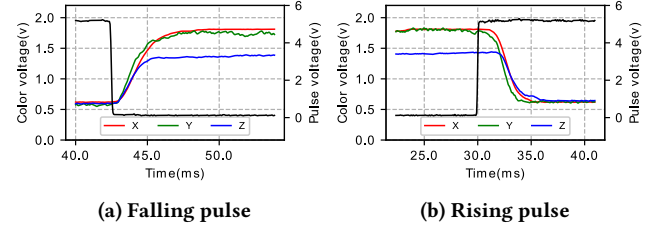
[3]Falling pulses are slower than rising pulses. With rising pulses, the re-alignment is forced by an electric field, while with falling pulses, only the internal (low) torque changes the orientation of the liquid crystal molecules.

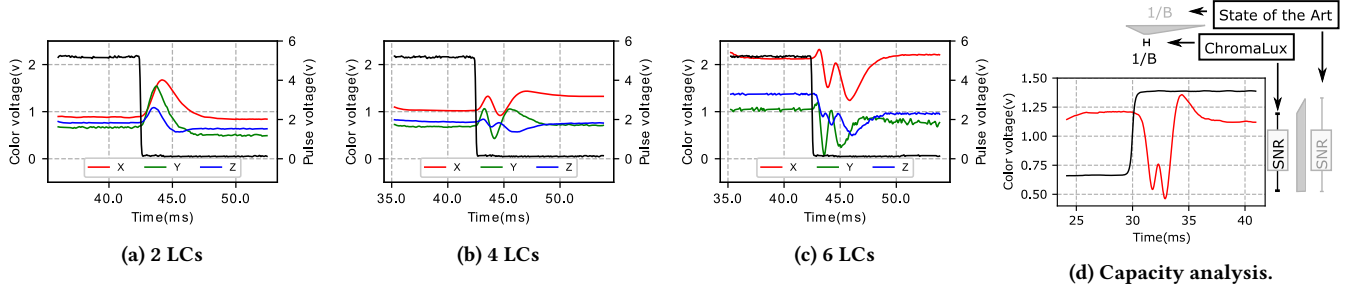(a) 2 LCs   (b) 4 LCs   (c) 6 LCs   (d) Capacity analysis.

Figure 9: Time responses for multiple LCs in series & capacity analysis.

thickness of the crystal layer, we cover a wider range of Gamma values. For example, with two cells, we cover an approximate Gamma range of [150, 500], and with six cells, the range is around [300, 1500]. The numerous peaks and valleys present in the transient state imply that, in the multi-cell case, two nearby points can provide a much higher contrast (SNR) compared to the *same* two nearby points in the single-cell case.

Second, the duration of the transient state remains the same for any number of cells. Note that the period of the transient states in Figure 8 and Figure 9 is around 5 ms for all cases. It would not be helpful if the transient state exposed peaks and valleys at the cost of an increased transition period. Even though the morphology of the transient state changes with a different number of cells, *its period remains the same*. This occurs because we control the LCs in parallel. In principle, the thicker the cell, the longer the time required to switch between states. Thus, in terms of switching speed, it is better to increase the thickness by using n cells (each with thickness w), instead of using a single (slower) cell with thickness $n \times w$.

Key insight: Increasing the thickness of the transmitter by stacking cells exposes a transient state where we can achieve a high switching speed between nearby points at a higher contrast compared to a single cell with the same modulation points.

3.3 Analyzing the channel's capacity

A fundamental goal for any wireless communication system is to increase its capacity. With LCs, the channel capacity is determined by their contrast and switching speed, but maximizing these two parameters represents opposing design goals. Thus, a crucial question is: if one has to choose, what is preferable in an LC, higher contrast or faster speed? Having a deep understanding of this trade-off is key to maximize the capacity of ambient-light links.

We use the well-known Shannon–Hartley theorem to anchor our discussion, $C = B * \log_2(1 + SNR)$. As shown in Figure 8, existing LCs are designed to maximize contrast (SNR) by covering the lowest valley (black) and the highest peak (white) in the theoretical response. This focus on contrast (SNR) as opposed to switching speed (B) makes sense for human-centric applications because human eyes have a slow frequency response. For wireless communication, however, preference must be given to the switching speed (B) because it increases the capacity linearly while the contrast (SNR) only gives a logarithmic improvement. Due to this reason, our focus will be on increasing the bandwidth of ChromaLux. As shown in Figure 9d, the key idea of ChromaLux is to trade a bit of SNR (using a single cell as the baseline) for a major gain in bandwidth.
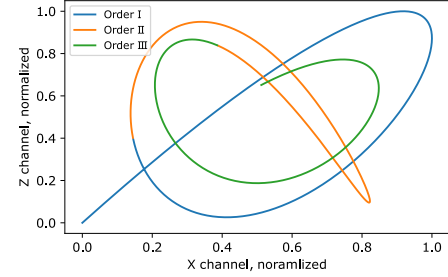

Figure 10: Theoretical constellation

4 A PRETZEL CONSTELLATION

As described in the prior section, adding LCs brings together more peaks and valleys within the transient state, which increases the bandwidth because the period between consecutive extremes is reduced. Thus, one may think that stacking as many LCs as possible would be the best approach to increase the bandwidth. But that is not the case. To understand the constraints of the transient state, we will first describe the differences between an ideal and a practical transmitter, and then propose a constellation to guide the selection of the number of cells and symbols.

An ideal transmitter. In theory, an ideal transmitter consisting of multiple LCs would cover a Gamma range from close-to-zero to a high value. The close-to-zero birefringence value (equivalent to an almost vertical radial line in the Michel Levy chart) would mean that the transient state includes the first valley and peak in the theoretical response, which provides the highest contrast (similar to using a single cell). The high birefringence value would allow us to compress multiple peaks and valleys inside the transient phase, reducing the switching speed amongst symbols (high bandwidth).

A practical transmitter. In practice, the minimum birefringence value in off-the-shelf cells is too high to include the first valley of the theoretical response once multiple cells are stacked, cf. Figure 7. Adding cells is beneficial, but for every cell we add, the spectrum moves further into the right side of the theoretical response (Figure 5), where the contrast of the signals decreases. In the next subsections, we provide a theoretical framework to guide the selection of (i) the number of cells that optimizes the morphology of the transient state, and (ii) the best region within the transient state to place our symbols.

4.1 Optical domain

For traditional RF and VLC systems, there are established methods to design the symbol space. The most common approach is to use

constellation diagrams that are independent of time. In order to create a time-independent constellation that connects theory with practice for ChromaLux, we plot the Z versus X channels for (i) the theoretical response, where the channels are a function of Gamma, and (ii) the empirical time responses, where the channels are a function of time[4].

The theoretical constellation is depicted in Figure 10, which looks like a pretzel. This graph is obtained by plotting the (X, Z)-pairs of the data underlying Figure 5. Within a constellation, the aim is to place symbols as far apart as possible from each other to maximize the signal-to-interference-plus-noise-ratio (SINR). However, contrary to the standard constellations used for RF or VLC, where symbols can be placed anywhere, we can *only* place symbols over the depicted curve. The constellation presented in Figure 10 is theoretical and *complete* up to the third order (plotting further orders would continue the trend inwards). In practice, ChromaLux will only see a subset of the constellation depending on how many cells we use. Figure 11 presents the partial constellation views obtained with 1 and 3 cells for falling and rising pulses. The rising pulses move in a counter-clockwise direction, and the falling pulses in a clockwise manner. Each one of these plots covers a subsection of the theoretical constellation, starting from the first order.

Our theoretical and empirical constellations provide an important design guideline regarding the number of cells that should be used. Adding too many cells pushes the constellation domain inwards, which would lead to tightly coupled symbols (low SINR). While adding cells, the designer should try to remain in the lowest possible order (most outward) to maintain a high SINR. In ChromaLux, we aim for the first intensity peak (Γ=250nm, see Figure 5) to be within the spectrum of our LC cell stack.By stacking cells, we move away from the first valley (black); hence, we should not miss the first peak (white) because that provides the second highest contrast in the theoretical response. In the next section, we will see that six cells is the optimal number for the type of LC we consider.

4.2 Time domain

In traditional constellations, the amount of time required to move between any pair of symbols is the same. That is not the case for LCs. The ChromaLux constellation has two important differences. First, the time to move between points changes depending on the chosen pair. For example, moving between symbols at the edges of the transient state –the "start" and "end" points of the constellations in Figure 11– can be one order of magnitude longer than moving between symbols in consecutive extremes. Second, the direction of movement matters. Moving during a falling pulse is slower than moving on the opposite direction (rising pulse).

It is important to recall that LCs behave almost like capacitors. Discharging a capacitor follows an exponential decay in time (e^{-t}) and its charging follows a ($1-e^{-t}$) trend. To connect these equations with our constellation, let us define three symbols in Figure 11d and their (approximate) counterparts in Figure 10. The symbols in the empirical constellation can be mapped to time and the symbols in the theoretical constellation can be mapped to Gamma values. If

(a) 1 LC: Falling pulse   **(b) 1 LC: Rising pulse**

(c) 3 LC: Falling pulse   **(d) 3 LC: Rising pulse**

Figure 11: Constellation diagrams for multiple LCs.

Figure 12: Gamma versus time

we plot the Gamma versus time curves of those symbols, we obtain Figure 12. This plot shows that, from a bandwidth perspective, not all symbols are born equal in our constellation. Due to the exponential trends, the symbols that appear at the beginning of a pulse are preferred because they are more compact in time, but there is an undesirable trade-off: the slow symbols appearing at the tail of the falling pulse are the fastest symbols in the rising pulse and vice-versa. In the next section, we will analyze this trade-off further to select our final symbols.

The unique temporal properties of our constellation provide an important design guideline for the following scenario: If the system needs to transmit multiple symbols (4, 8, or more), is it better to use a single-pixel transmitter transmitting all symbols? or, a set of multi-pixel transmitters, with each pixel transmitting a pair of symbols? The answer is that it is better to implement a multi-pixel transmitter with two symbols per pixel. This is because a single-pixel transmitter has a key drawback: the bandwidth can be reduced significantly if multiple symbols are transmitted because the time taken to switch between different symbols at the extremities can

---

[4]Note that in principle, the constellation should be a 3D space covering the XYZ dimensions, but that is hard to visualize. The XYZ color space has the nice property of projecting most colors onto the 2-D space captured by the X and Z channels. The Y channel is called the luminosity.
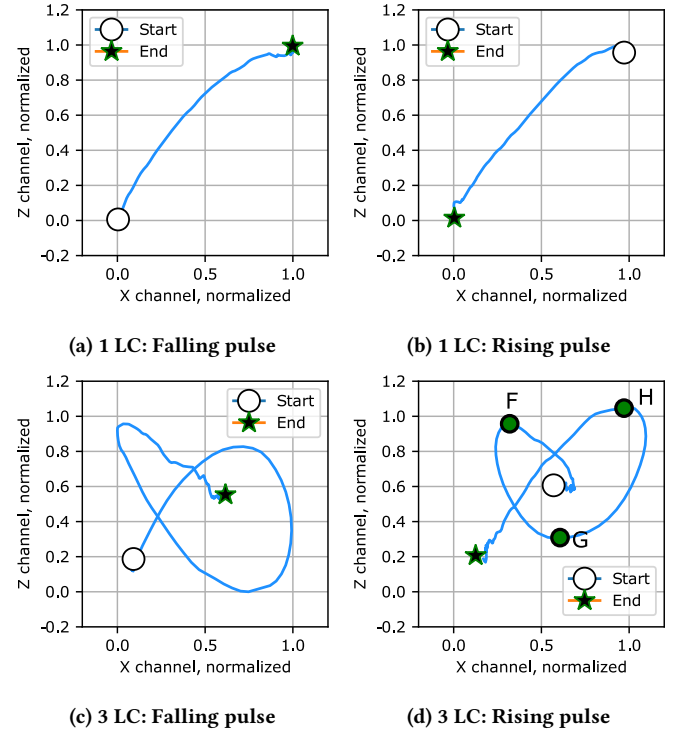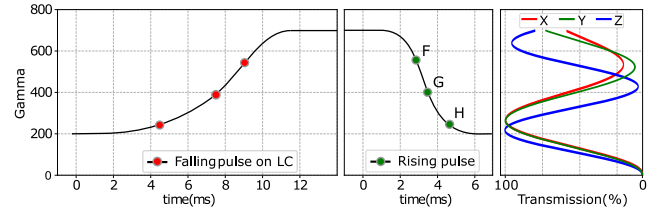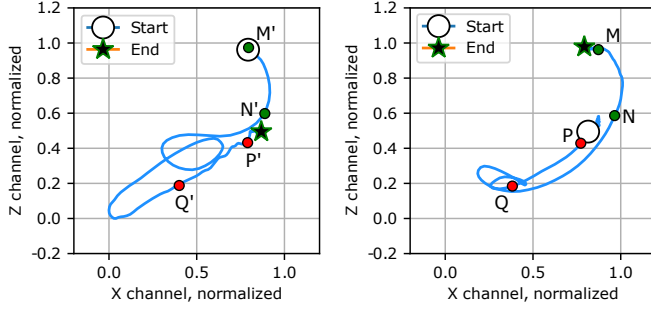
(a) 6 LCs: Falling pulse **(b) 6 LCs: Rising pulse**

Figure 13: Constellations for six LCs

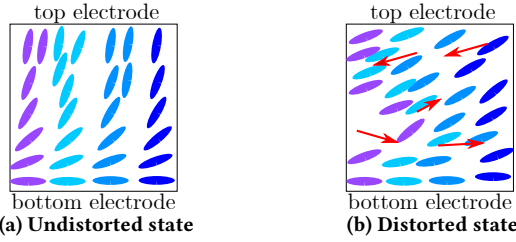**(a) Undistorted state** **(b) Distorted state**

Figure 14: The cross-section of an LC cell showing the back-flow effect. The colors of the molecules are used to highlight their distorted displacement in the transient region, and the red arrows show the liquid flow directions. A more fine-grained analysis is presented in [16].

be too long. For example, for the falling pulse in Figure 12, the time difference between symbols F and H is much longer than between symbols F and G. If we use a multi-pixel transmitter, each pixel can transmit one pair of *nearby* symbols, thereby increasing the system's bandwidth.

Given that our analysis in subsection 3.3 shows that increasing bandwidth is more relevant than increasing the number of symbols, our focus will be on designing a fast single-pixel transmitter modulating two symbols.
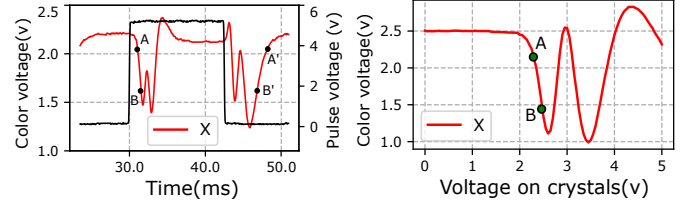
5 COMMUNICATION SYSTEM

The idea behind faster modulation relies on the fact that by stacking liquid crystals, we can get a distinguishable contrast between on/off states without waiting for full transitions. In this section, we describe the approach we take to define the number of LCs, the symbols, and the modulation method.

5.1 Number of cells and symbol selection

Selecting the right number of cells is a delicate balance between increasing the spectrum of the transient state and decreasing the contrast. As most of the LC cells available on the market lack important optical and electrical specifications, we first mention how to select symbols empirically and then theoretically in case the specifications are known.

Empirical method. In order to maximize the contrast, an important extremum to capture is the highest peak (white) in Figure 5, given that using multiple cells excludes the lowest valley. Figure 7 shows that using six cells allows us to achieve that balance. The

(a) Dynamic pulses. **(b) DC voltage**

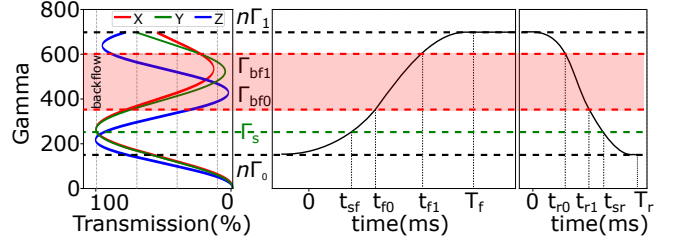**Figure 15: Communication symbols**

Figure 16: Theoretical Framework. The theoretical response (left plot) can be used to obtain the valid range of Gamma values, and the capacitance response (center and right plots) can be used to map the Gamma values to time values.

spectrum starts around the white peak and continues to cover several orders. To select the best pair of symbols for this spectrum, we use the constellations shown in Figure 13. Notice that, for six cells, the empirical constellation is a highly distorted version of the theoretical one. Those major distortions start to appear when using four or more cells of this particular type. Note that when we use three cells, cf. Figure 11, the theoretical and empirical constellations have a closer resemblance. We hypothesize that this distortion is due to the "backflow effect" of liquid crystals [16]. When an electric field is applied, the LC molecules do *not* re-align in an orderly manner, as shown in Figure 14a. In fact, the electric field creates a temporary internal flow, similar to swirl, as depicted in Figure 14b. The more LC cells we use, the more visible this effect becomes due to the compounding effect of multiple backflows occurring in parallel.

The backflow effect is a transient phenomenon that dissipates close to the end states. Hence, the beginning and end of the constellations show a stronger symmetry, which is desirable for modulation. In Figure 13, those symmetric regions are present between points P/P'– Q/Q' and N/N' – M/M'. We decide to use symbols P/P' and Q/Q' because they provide a slightly better SINR. Each symbol maps to an (X,Y,Z) tuple in the time response in Figure 9c. We select channel X as our carrier, as there is not much difference between channels X and Y, and channel Z has a lower peak-to-valley difference. The final symbols A and B are shown in Figure 15a (channel X) on top of a sample rising and falling pulse.

Theoretical method. The approach presented in this paper is largely empirical because off-the-shelf LCs do not provide detailed optical and electrical parameters. A theoretical framework can be used to determine the system's symbols if the LC's datasheet specifies the following parameters: the cell's thickness d, the minimum and maximum birefringence values (Δn_{min} and Δn_{max}), and the

electric capacitance C_e. A theoretical procedure consists of the following steps:

Step 1: Obtaining optimal number of cells (n). Following the path difference (Γ) defined in Equation 2 and denoting $\Gamma_0 = \Delta n_{min} \times d$ and $\Gamma_1 = \Delta n_{max} \times d$ in nm, the spectrum $[\Gamma_0, \Gamma_1]$ is covered by a single cell. If we stack n cells, the new range of Γ is $[n\Gamma_0, n\Gamma_1]$. The best value for n is the highest number that still covers the first peak (because it provides the highest contrast). If n grows beyond that value, we miss that important (white light) peak. A theoretical optimal range $[n\Gamma_0, n\Gamma_1]$ is depicted on the left side of Figure 16.

Step 2: Discarding the asymmetric backflow region. The range defined in Step 1 includes the distorted region caused by the backflow effect. To identify and avoid that region, methods such as those described in [16] can be used to simulate the rising (falling) pulse for time periods $t_r(t_f)$. That simulation would pinpoint the region where the distortions are so high that no symmetry is maintained in the constellation plots. The Gamma range capturing the undesirable backflow (bf) region $[\Gamma_{bf0}, \Gamma_{bf1}]$ is highlighted in red in Figure 16.

Step 3: Mapping Gamma values to time values. Until now, the theoretical framework has focused only on Gamma values (left plot in Figure 16). All these Gamma values can be mapped to time values using the time response defined by the electric capacitance C_e (center and right plots in Figure 16). For example, Γ_s, selected as our symbol, can be mapped to t_{sf} and t_{sr}[5]. The experimental counterpart of the region between Γ_{bf0} and Γ_{bf1} is the line between Q and N (or Q' and N' equivalently) in Figure 13. Thus, we have to select symbols from the following set:

$$[n\Gamma_0, \Gamma_{bf0}] \cup [\Gamma_{bf1}, n\Gamma_1]$$

Due to the lack of specifications for our LC cells, we determined t_{r1} and t_{f0} empirically, using the pretzel graphs shown before. We will use this timing information in the next section to devise our modulation scheme.

5.2 Modulation

The unique properties of the transient state require a different modulation method compared to those found in the SoA. First, we will describe why existing methods based on two voltage levels do not work, and then, we present our three-voltage-level approach.

5.2.1 Two voltage levels. The most common approach to modulate LCs is to map a voltage level to a symbol. Considering that the voltage controls the birefringence (and Gamma) values of LCs, one could use static DC voltage levels to keep the LC in state A or B. Figure 15b depicts the X channel values when we apply a DC voltage in steps of 0.1 from 0 to 5. This DC response is an undistorted, stable version of the dynamic rising and falling responses in Figure 15a. Symbols A and B are located at 2.2 V and 2.4 V, respectively. The problem of using a direct OOK modulation with those voltages is that the system would have slower transitions than when the voltage swing is 5 volts.

To overcome the slow (exponential) transitions between voltages, another option is to emulate the 2.2 V and 2.4 V via high-frequency pulses between 0 and 5 V. This broader voltage range provides faster

[5]Note that the theoretical response and the time capacitance plots in Figure 16 are only dependants on the optical/electrical specifications of a single cell. Only the shift upwards in the theoretical response (left plot) depends on the number of cells.
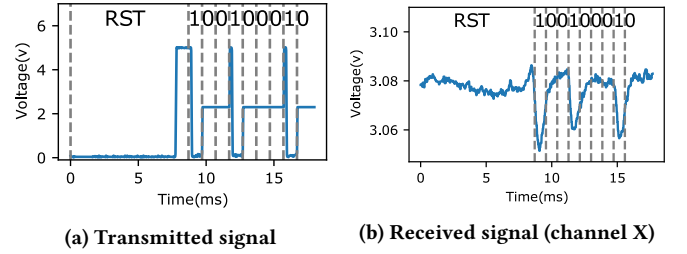

(a) Transmitted signal **(b) Received signal (channel X)**

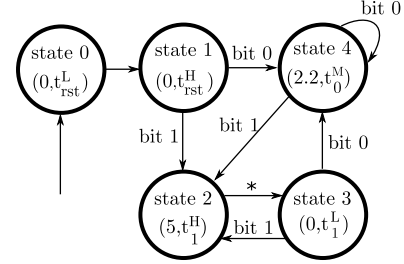**Figure 17: Sample signals at transmitter and receiver.**

Figure 18: The state machine of the transmitter.

transitions between the chosen symbols. An emulated DC value is equal to the maximum voltage (5 V) times the duty cycle of the pulse train. For our case, a 10 kHz signal would be sufficient to create the desired voltage levels. The drawback of this approach, compared to using the DC option, is that the high-frequency oscillations increase the noise level and power consumption.

5.2.2 Three voltage levels. To combine the fast transitions of the [0,5] V range and the stability of DC voltages, we propose to use three voltage levels: 0, 2.2, and 5. A sample waveform of the transmitted and received signals are shown in Figure 17. To send bit 0, we use the 2.2 V to hold the LC in state A. The receiver will see bit 0 as a noisy 'flat' signal. To send bit 1, we generate the transition A-B-A by using a voltage sequence of 5-0. If these two voltages are kept for the proper duration, then the receiver will see bit 1 as a "V" shaped signal. The state machine of our transmitter is presented in Figure 18. Each state represents a tuple (V, t), where V denotes the voltage level and t the amount of time spent in that state.

State 0: Considering that LCs (like capacitors) can have random charges stored on them when disconnected. At the start-up, we need to reset (RST) the voltage by keeping it at 0 for a period long enough to reach the steady-state: t_{rst}^L = 8 ms. This time has to be longer than T_f shown in Figure 16.

State 1: The second part of the *reset* uses a 5 V signal for a period of t_{rst}^H = 0.9 ms. This duration can be measured from Figure 15a and represents the amount of time required to reach symbol A with a rising pulse. If we look at the theoretical graph in Figure 16, t_{rst}^H is equal to t_{sr}, where the maximum of channel X occurs. At this point, the device can start transmitting bits.

State 2: If at the end of the reset state, the transmitter has to send a "1", a transition has to be made from point A to B. This transition represents the '\' part of the V shape seen in the receiver. A 5 V signal is applied for a duration of t_1^H = 0.2 ms so the LCs can reach point B. In Figure 16, t_1^H is equivalent to $T_r - t_{sr}$. After this period, the transition to State 3 is made automatically.

State 3: A 0 V is applied for the duration of t_1^L = 0.8 ms. This duration is the time needed to get from B' to A', which is the '/' of the V shape for the symbol "1". In Figure 16, we have to apply a low pulse with the duration of t_{sf}. When the time for this step is up, the transmitter can send a new bit.

State 4: If the next bit to be sent is a 0, the only thing that the transmitter needs to do is to keep the LC at point A. To make this happen the middle voltage (2.2) is applied on the LC stack for a period t_0^M = 1 ms.

5.3 Demodulation

To demodulate the received signal, we take the steps below. Our packet structure has a reset phase, a bit-1 for synchronization, and 84 bits of data after that.

Step 1: The receiver constantly measures the signal's mean and noise variance with a moving window of size 4 ms (equivalent to the length of four bits).

Step 2: If the variance changes by a factor of X or more with respect to the noise variance measured during the idle period, the receiver enters a phase-lock phase.

Step 3: Given that the first bit after the reset phase is a "1", the receiver looks for the first minimum. This enables the receiver to lock onto the phase of the transmitter. After that, we start decoding data bits.

Step 4: If the variance of the received signal during a symbol period is lower than a threshold (determined by the noise floor of the LC, which is comparable to the channel noise), the symbol is demodulated as a "0". If the variance is higher than the threshold, we use the maximum and minimum values in the window to build a reference "V" shape, and a matched filter using Pearson correlation determines if the symbol is indeed a bit 1.

Step 5: Every time a symbol "1" is found in the incoming signal, the receiver's phase is corrected to account for small drifts and mismatch in symbol length, which are caused by the fact that LCs are operated in an unstable region. We cannot perform any such drift correction when a long series of "0" is received, but for the packet size we use (84 bits) no major synchronization issues surfaced.

6 PLATFORMS

We designed PCB and 3D-printed enclosures for the transmitter and receiver, both equipped with batteries.

6.1 Transmitter

We use an STM32L031K6 microcontroller with four different voltage outputs. When using multiple cells, the output can act as a high capacitive load, which may render the circuit unstable. In our implementation, the maximum capacitance of the liquid crystal cells is 72 nF, which does not impose any problem. We use a basic op-amp (OPA2325) between the microcontroller output pins and the six commercial LC shutters. The transmitter's enclosure allows for both ambient and artificial light to be used. For artificial light, we use the flashlight of a smartphone, and for ambient light, a metal surface acts as a light reflector. We programmed the platform to send always the same packet: "HELLO WORLD\0".
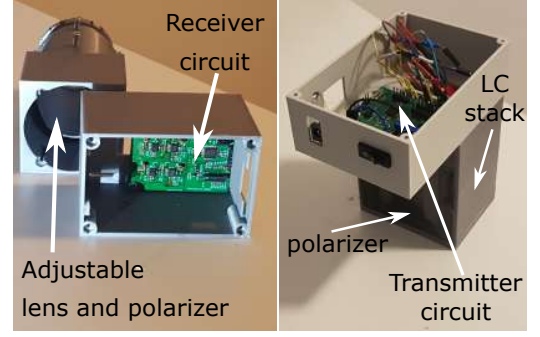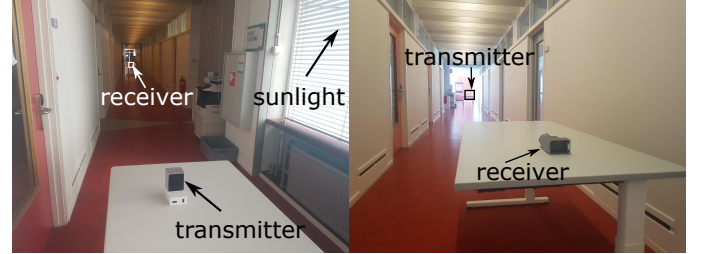

Figure 19: PCBs & enclosures: TX(left), RX(right)

(a) Transmitter's view   **(b) Receiver's view**

Figure 20: Long range experiment setup

6.2 Receiver

We use a MAZeT true color sensor. The response of this color sensor conforms to the CIE 1931 standard. An arbitrary number of amplifier stages can be used to get a desired amplitude for the signal; we use three stages. A transimpedance amplifier is used as the first stage (47 kOhm transimpedance resistor). We can change the amplification factor of the signal based on the distance to the transmitter, 31x gain for low range, and 143x for long-range. To make the platform able to communicate over long distances, we use a lens. The lens reduces the field of view, but it significantly increases the signal to noise ratio. The lens is adjustable, so the platform can be used from very short distances (~ 1 meter) to long distances (~ 50 meters). We make use of a well-known concept in optics called the "hyperfocal distance," which allows foreground and background to appear reasonably sharp. In our work, the position of the lens is fixed for any range beyond 15 m (approximately). That is, we do *not* need to adjust the lens for any range beyond that; we only calibrate the lens for ranges shorter than 15 m.

7 EVALUATION

To evaluate the platform, we look into two different scenarios. For natural light, we put our transmitter on a long aisle close to a window, as in Figure 20. During our evaluation, the light intensity was between 3 kLux (partly cloudy day) to 6 kLux (clearer day). For artificial light, we put our platform in a room and use a flashlight that radiates between 300 to 700 Lux depending on how close we place the flashlight to the transmitter. It is important to remark that our system does not cause any flickering effects. Similar to other studies [9, 22, 25, 27], our modulation is based on changes in polarization, which are not visible to the naked eye.
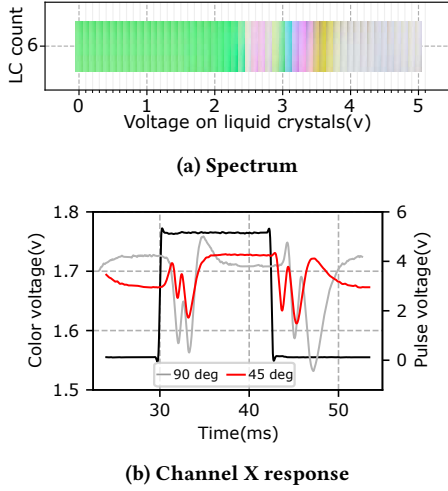
(a) Spectrum

(b) Channel X response

Figure 21: 6 LCs: Rotation on roll axis at 45°

7.1 Data rate, range, and rotation

We use two different settings for the data rate: 1 kbps and 1.25 kbps. For each data rate, we send forty packets at each distance. A packet consists of 84 bits of data and one bit for synchronization. We will present the average and standard deviation of the measured BER of the total transmitted bits.

The 1 kbps data rate is obtained using the default A and B symbols shown in Figure 15a. For a data rate of 1.25 kbps, we bring those two symbols a little closer (modifying the corresponding voltages according to our modulation method), which increases the switching speed, but reduces the contrast.

Figure 22a presents the results with artificial light, where we obtain a range of up to 5 m with 1.25 kbps and 10 m with 1 kbps while maintaining the BER below 1%. An intensity of 300 to 700 lux is a relatively low value (standards suggest at least 500 lux for desk related work). Sunlight can provide values between a few klux (cloudy day) to several 10 klux (very sunny day). To test the performance of our system with natural light, we set it up in the hallway of our lab, see Figure 20. Figure 22b presents the results. We now achieve a 50 m range at 1 kbps with an average BER below 1%. Compared to the SoA, this range is 20 times longer than single-pixel systems providing a similar 1 kbps rate [26], and the data rate is 10 times higher than our prior single-pixel system that achieves a long range with sunlight (65m with 10k+ lux), but transmits only at 80 bps [6].

To test the resilience of our system to rotations around the roll axis, we modify the relative alignment of the analyzer from 0 to 45°. Figure 21a shows the color spectrum seen out of the six cells when the analyzer has a relative angle of 45°. Compared to Figure 7, the spectrum is shifted to the left. Figure 21b shows the X channel response for this configuration, where we can see that the response shifts in time. So long as the symbols A and B remain in the right slope, the system works, but if the shift is too far, the misalignment will break the link. Figure 22c shows the results with different rotation angles and two different ranges (under artificial lighting); beyond 30° the ChromaLux link breaks.

7.2 Energy consumption

To measure the power consumption, we divide our system into two parts: the optical frontend (transmitter's LCs and receiver's color sensor) and the processing part (microcontroller for both). The power consumed by the LCs is so low (sub mW) that we could not measure it accurately. Thus, we use the well-known equation that considers their almost perfect resemblance to capacitors, assuming that the bit pattern consists of an equal number of zeros and ones: $P = CV^2 f$, where $f = \frac{\text{bit rate}}{2}$, V is the weighted average of the middle voltage and 5V, and C is the capacitance of the LC stack (13 nF for our cells). The tables below show the power consumption for our platform. Similar to all other backscatter systems, the cost of the LCs is negligible. The bulk of the power is consumed by the processing and amplification at the receiver, a little over 100 mW in total.

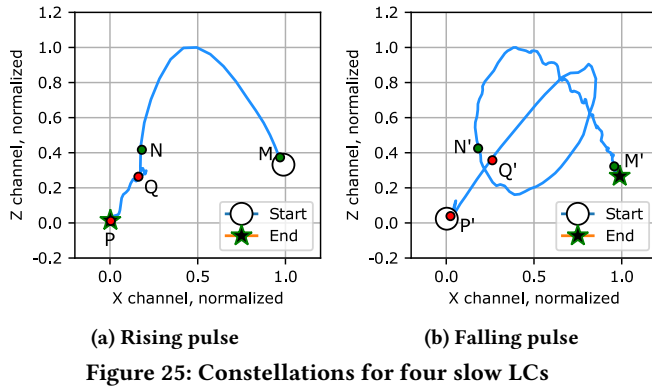| Transmitter @ 1 kbps		
Component	Operating voltage	Power consumption
LC stack	$0, V_{mid}, 5$	0.166 mW
Microcontroller	3.3	27.3 mW

Receiver		
Component	Operating votage	Power consumption
Sensor amplifiers	3.3	72.6 mW
Microcontroller	3.3	39.6 mW

7.3 Generality of the solution

The method proposed in this paper can be applied to any type of TN liquid crystal cell, which is the most well-known and inexpensive type). To show that, we use our framework on another LC, which has a bigger surface area [2], and thus, is inherently slower. We utilize our constellation analysis (section 4) to define the optimal number of cells (four in this case) and the optimal position of symbols, then to adjust the modulation accordingly, we utilize the methods presented in section 5.

Figure 23 shows the temporal response for one cell. The rising and falling times are around 6 and 40 ms, significantly slower than the ones used for our first LC at 3 and 4 ms, respectively (Figure 8). Figure 24 shows the responses for the optimal number of slow cells (four). Note that the transient state exposes peaks and valleys with high contrast, but they do not look like mirror images of each other, which was the case for the first LCs (Figure 15a). This asymmetry is due to the bigger difference between the falling and rising times. This high asymmetry requires a careful analysis of the constellations for this setup, shown in Figures 25. Considering the backflow effect of LCs, only two regions are suitable for modulation; one is between points M and N (and respectively M' and N' in the falling response), and the other is between points P and Q. As we are using channel X to transmit data, points M and N have a higher SINR, compared to points P and Q, and thus, we use them.

After fixing the middle voltage, for bit 0, the modulation and demodulation remain the same for the other type of liquid crystals. Figure 22d shows the results with artificial light (short-range with 700 lux). Observe that even though the total response time (falling + rising time) for a single cell is around 50 ms (~20 bps with basic OOK), ChromaLux obtains a 25× higher data rate (500 bps). It is important to note that studies like PassiveVLC [26] and LuxLink [6]

(a) Fast LCs:
short range 300 to 700 Lux

(b) Fast LCs:
long range, 3 kLux to 6 kLux

(c) Fast LCs:
Rotations on roll axis

(d) Slow LCs:
short range, 700 Lux

Figure 22: Evaluation results.

(a) 1 LC: Rising pulse

(b) 1 LC: Falling pulse

Figure 23: Empirical response for one slow LC

(a) 4 LC: Rising pulse

(b) 4 LC: Falling pulse

Figure 24: Empirical response for four slow LCs

(a) Rising pulse

(b) Falling pulse

Figure 25: Constellations for four slow LCs

do not use such slow LCs, but faster ones similar to the ones in our first batch of experiments. Thus, ChromaLux shows that it can improve the performance of LCs that have not even been considered in the backscatter community for being too slow.

8 RELATED WORK

The description of the SoA focuses on the area of *passive* communication with ambient light. A summary of the comparison between ChromaLux and the most related studies is presented in a table at the end of this section. We divide the SoA into four main domains.

Single-pixel. The idea of using (retro)reflectors for communication was first proposed in smart dust via mechanical oscillations [24]. More recently, LCs were proposed to avoid the need for mechanical movements. Retro-VLC [14], Passive-VLC [26], and LuxLink [6] are all platforms using a single LC cell at the transmitter and a single photodiode at the receiver. Retro-VLC and Passive-VLC achieve 500 bps and 1kbps, respectively, at short ranges (∼2 m), and LuxLink exploits sunlight to achieve 80 bps at long ranges (65 m). All these studies exploit only the default monotonic range in LCs. ChromaLux uses more than one LC to create a single-pixel transmitter, exposing a novel transient state that allows us to match the long range (50 m) and high data rate (1 kbps) of existing single-pixel systems simultaneously.

Multi-pixel. The focus of our work is on a single-input single-output system (SISO). Other studies have explored SIMO and MIMO methods to increase the capacity of backscatter systems with notable results. Using a novel differential reception method with two photodiodes and a backscatter panel consisting of 36 LCs, RetroI2V–a SIMO approach–achieves a performance similar to ChromaLux: 1 kbps at 80 m with less than 1% BER and a ±15° resilience to polarity rotation [22]. In a more recent study, RetroTurbo–a MIMO approach–also utilizes two photodiodes at the receiver, but with 64 pixels on the backscattering surface [25]. Exploiting fast shutters, they create constellations that can achieve 8 kbps at 7 m with less than 1% BER. These studies are valuable and orthogonal to ChromaLux. We do not exploit multi-sensor/pixel methods, and they do not use transient states. These multi-pixel approaches still rely on monotonic transitions. Increasing the performance of ChromaLux with multi-pixel/sensor methods is part of our immediate future work. Pixelated-VLC follows a similar approach, but with a MISO system [15]. Using three shutters, they utilize Pulse Amplitude Modulation to achieve 600 bps at 2 m.

Color-based. Several studies have used *passive* optical materials to create color patterns based on birefringence. Pixel [27] and Poli [9] add a dispersor to an LC to shift the color spectrum, and use color shift keying to transmit data to a camera. This achieves resilience for relative rotations between the tag and smartphone, but the studies do not identify the presence of a transient state. They only use the end-states, and thus, achieve a low data rate and short range, 14 bps at 10 m for Pixel (using a single shutter) and 72 bps at 10 m for Poli (using three shutters with three LEDs). Other studies do not use LCs, only polarizers and dispersors to create tags that radiate various color patterns. These studies cannot transmit data, but the optical tags provide valuable information. PolarTag

Comparison with the state-of-the-art (SoA)						
	Light source	Data rate	Range	Tx Power	Tx pixel count	Receiver
RetroVLC[14]	LED lamp	10 kbps (down)/0.5 kbps (up)	2.4 m	234 µW	1	Photodiode
PassiveVLC[26]	LED lamp	2.5 kbps (down)/1 kbps (up)	2 m	525 µW	1	Photodiode
PIXEL[27]	LED/Ambient light	14 bps	10 m	1 mW	1	Camera
RetroTurbo[25]	LED lamp	8 kbps	7.5 m	0.8 mW (LC) 4 W (Sys.)	64	Photodiode
LuxLink[6]	Ambient light	80 bps	4.5 to 65 m	30 mW	1	Photodiode
ChromaLux	Ambient light	1 kbps	1 to 50 m	27.3 mW	4 to 6 in series	Color sensor

creates colorful patterns that are similar to QR codes, but invisible to humans and provide better performance [18]. Based on the same principle, Tian et. al. [19], place tags on ceiling lights to radiate a chess-like pattern of colors over the floor. The color patterns are decoded by a sensor to enhance the localization accuracy of IMU-based systems. RainbowLight uses tags that change in color based on the angle-of-view [12]. The tags are visible for people, but they can achieve localization accuracy below 5 cm. None of these passive systems use LCs to transmit data, and hence, they did not uncover the existence of the transient state.

Other related studies. Some works have looked into exploiting sunlight for vehicle-to-infrastructure communication without using LC cells or other passive optical components [7, 23]. The basic idea is similar to a barcode reader. Big barcodes are placed on the surfaces of vehicles, and as they move, the changes in light intensity are captured by photodiodes on the street. Those systems are simple and low-cost, but they require mobile objects and achieve a limited data rate at short ranges, 120 bps at 4 m.

9 DISCUSSION

In this section, we elaborate on some difficulties that arise as a result of stacking LC cells in series.

9.1 Carrier signal attenuation

In ChromaLux, we stack off-the-shelf LC cells because we cannot manufacture a cell with the desired optical properties. The main disadvantage of stacking LCs is that instead of using two glass electrodes, we use $2 \times n$. To calculate the attenuation, we can do the following numerical analysis. The glasses used in LC cells are coated with Indium-Tin-Oxide (ITO), which is a transparent conductor. Some ITO layers can transmit a maximum of 90% of visible light [3]. Hence, the transmission factor caused by the six cells is about 0.3 . We measured the transmission factor of our cells and found that six cells lead to a value of 0.37, which is a little bit better than the theoretical result. This attenuation reduces the range by approximately 40% [21]. That is, instead of reaching 50 m, designing a custom cell with only two glass electrodes could reach a distance of 80 m.

9.2 Variation of LC cells

Due to inaccuracies in the manufacturing process, it is possible for LCs to have different optical responses, and these differences could distort the modulation of symbols. To evaluate this aspect, we test four batches of six LC cells each. The six cells are different combinations taken out of a set of eleven cells.
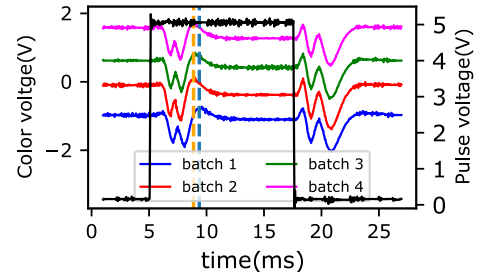

Figure 26: Characterization of different LC batches.

The results are shown in Figure 26, which captures the optical responses in the X channel for a 40 Hz pulse. We can observe that, except for batch 1, all the other batches have a strong alignment. Batch 1 has a delay of around 0.5 milliseconds. This delay would not affect the modulation of the 'flat' bit 0, but it could distort the shape of the bit 1. Instead of a ∨ shape, the bit 1 would have a ⋎ shape. The system would still be able to demodulate the bit 1, but if the delay increases further, the ⋎ shape may start becoming a flat line, rendering the demodulation futile. If instead of a delay, the signal would come ahead of time. The ∨ shape would turn into a W shape. The system would still be able to decode a bit 1; however, the corrected phase would be off by one-forth of the symbol length. If the signal keeps on starting earlier, the modulation of the bit 1 would be done inside the backflow region, which may create undecodable distortions. To overcome this problem, a feedback loop can be created at the transmitter to fine-tune the modulation parameters (timers) in order to adjust to the observed delays.

10 CONCLUSION

In this work, we looked into a fundamental assumption made on backscatter communication: the idea that changes in light intensity between the end states of LCs follow a monotonic function. Based on first principles, we showed that LC-based transmitters can be designed to have non-monotonic transient states that can be exploited to increase the link's capacity. Compared to existing single-pixel systems, ChromaLux achieves simultaneously a long range (50 m) and a high data rate (1 kbps). The most important contribution of ChromaLux, however, is that it provides an initial framework for a principled design of ambient backscattering.

11 ACKNOWLEDGEMENTS

REFERENCES

[1] 2020. Active 3D glass. https://bit.ly/31hKJ4m.

[2] 2020. Active 3D glass. https://www.adafruit.com/product/3330.

[3] Hadi Askari, Hamidreza Fallah, Mehdi Askari, and Mehdi Charkhchi Mohm-madieyh. 2014. Electrical and optical properties of ITO thin films prepared by DC magnetron sputtering for low-emitting coatings. *arXiv preprint arXiv:1409.5293* (2014).

[4] Markus Bauer. 2017. Michel-Levy chart. https://github.com/markus-bauer/calculated_Michel_Levy_Chart.

[5] PD Berezin, IN Kompanets, VV Nikitin, and SA Pickin. 1973. The orienting effect of an electric field on nematic liquid crystals. *Journal of Experimental and Theoretical Physics* 64 (1973), 599–607.

[6] Rens Bloom, Marco Zúñiga Zamalloa, and Chaitra Pai. 2019. LuxLink: creating a wireless link from ambient light. In *Proceedings of the 17th Conference on Embedded Networked Sensor Systems*. 166–178.

[7] Rens Bloom, Marco Zuniga, Qing Wang, and Domenico Giustiniano. 2019. Tweeting with sunlight: Encoding data on mobile objects. In *IEEE INFOCOM 2019-IEEE Conference on Computer Communications*. IEEE, 1324–1332.

[8] F. Donald Bloss. 2002. Optical Crystallography. Mineralogical Society of America Monograph Series, No. 5., 1999 ISBN 0939950499. *Journal of Petrology* 43, 3 (03 2002), 579–580.

[9] Chun-Ling Chan, Hsin-Mu Tsai, and Kate Ching-Ju Lin. 2017. POLI: Long-Range Visible Light Communications Using Polarized Light Intensity Modulation. In *Proceedings of the 15th Annual International Conference on Mobile Systems, Applications, and Services* (Niagara Falls, New York, USA) *(MobiSys '17)*. ACM, New York, NY, USA, 109–120.

[10] Vsevolod Fréedericksz and V Zolina. 1933. Forces causing the orientation of an anisotropic liquid. *Transactions of the Faraday Society* 29, 140 (1933), 919–930.

[11] Ye-Sheng Kuo, Pat Pannuto, Ko-Jen Hsiao, and Prabal Dutta. 2014. Luxapose: Indoor Positioning with Mobile Phones and Visible Light. In *Proceedings of the 20th Annual International Conference on Mobile Computing and Networking* (Maui, Hawaii, USA) *(MobiCom '14)*. ACM, New York, NY, USA, 447–458.

[12] Lingkun Li, Pengjin Xie, and Jiliang Wang. 2018. Rainbowlight: Towards low cost ambient light positioning with mobile phones. In *Proceedings of the 24th Annual International Conference on Mobile Computing and Networking*. 445–457.

[13] Tianxing Li, Chuankai An, Zhao Tian, Andrew T. Campbell, and Xia Zhou. 2015. Human Sensing Using Visible Light Communication. In *Proceedings of the ACM MobiCom*.

[14] Jiangtao Li, *et al.* 2015. Retro-VLC: Enabling Battery-free Duplex Visible Light Communication for Mobile and IoT Applications. In *HotMobile*.

[15] Sihua Shao, Abdallah Khreishah, and Hany Elgala. 2017. Pixelated VLC-Backscattering for Self-Charging Indoor IoT Devices. *IEEE Photonics Technology Letters* 29 (2017), 177–180.

[16] Alfeus Sunarso, Tomohiro Tsuji, and Shigeomi Chono. 2008. Molecular dynamics simulation of backflow generation in nematic liquid crystals. *Applied physics letters* 93, 24 (2008), 244106.

[17] Bjørn Sørensen. 2013. A revised Michel-Lévy interference colour chart based on first-principles calculations. *European Journal of Mineralogy* 1 (02 2013).

[18] Zhao Tian, Charles J Carver, Qijia Shao, Monika Roznere, Alberto Quattrini Li, and Xia Zhou. 2020. PolarTag: Invisible Data with Light Polarization. In *Proceedings of the 21st International Workshop on Mobile Computing Systems and Applications*. 74–79.

[19] Zhao Tian, Yu-Lin Wei, Wei-Nin Chang, Xi Xiong, Changxi Zheng, Hsin-Mu Tsai, Kate Ching-Ju Lin, and Xia Zhou. 2018. Augmenting Indoor Inertial Tracking with Polarized Light. In *Proceedings of the 16th Annual International Conference on Mobile Systems, Applications, and Services* (Munich, Germany) *(MobiSys '18)*. ACM, New York, NY, USA, 362–375.

[20] N.O. Tippenhauer, D. Giustiniano, and S. Mangold. 2012. Toys communicating with LEDs: Enabling toy cars interaction. In *Proceedings of the IEEE CCNC*. 48–49.

[21] Nikolaos Voudoukis and Sarantos Oikonomidis. 2017. Inverse square law for light and radiation: A unifying educational approach. *European Journal of Engineering Research and Science* 2, 11 (2017), 23–27.

[22] Purui Wang, Lilei Feng, Guojun Chen, Chenren Xu, Yue Wu, Kenuo Xu, Guobin Shen, Kuntai Du, Gang Huang, and Xuanzhe Liu. 2020. Renovating road signs for infrastructure-to-vehicle networking: a visible light backscatter communication and networking approach. In *Proceedings of the 26th Annual International Conference on Mobile Computing and Networking*. 1–13.

[23] Qing Wang, Marco Zuniga, and Domenico Giustiniano. 2016. Passive Communication with Ambient Light. In *Proceedings of the 12th International on Conference on Emerging Networking EXperiments and Technologies* (Irvine, California, USA) *(CoNEXT '16)*. ACM, New York, NY, USA, 97–104.

[24] Brett Warneke, Matt Last, Brian Liebowitz, and Kristofer SJ Pister. 2001. Smart dust: Communicating with a cubic-millimeter computer. *Computer* 34, 1 (2001), 44–51.

[25] Yue Wu, Purui Wang, Kenuo Xu, Lilei Feng, and Chenren Xu. 2020. Turboboosting Visible Light Backscatter Communication. In *Proceedings of the Annual conference of the ACM Special Interest Group on Data Communication on the applications, technologies, architectures, and protocols for computer communication*. 186–197.

[26] Xieyang Xu, *et al.* 2017. PassiveVLC: Enabling Practical Visible Light Backscatter Communication for Battery-free IoT Applications. In *MobiCom*. 180–192.

[27] Zhice Yang, Zeyu Wang, Jiansong Zhang, Chenyu Huang, and Qian Zhang. 2015. Wearables Can Afford: Light-weight Indoor Positioning with Visible Light. In *Proceedings of the 13th Annual International Conference on Mobile Systems, Applications, and Services* (Florence, Italy) *(MobiSys '15)*. ACM, New York, NY, USA, 317–330.

[28] Yang Zou, Jun Namkung, Yongbin Lin, Dan Ke, and Robert Lindquist. ts ,. Interference colors of nematic liquid crystal films at different applied voltages and surface anchoring conditions. *Opt. Express* 19, 4 (Feb ts ,), 3297–3303.